Quantum Dot in the Kondo Regime Coupled to Superconductors

M. R. Buitelaar, T. Nussbaumer, and C. Schönenberger*

Institut für Physik, Universität Basel, Klingelbergstrasse 82, CH-4056 Basel, Switzerland

The Kondo effect and superconductivity are both prime examples of many-body phenomena. Here we report transport measurements on a carbon nanotube quantum dot coupled to superconducting leads that show a delicate interplay between both effects. We demonstrate that the superconductivity of the leads does not destroy the Kondo correlations on the quantum dot when the Kondo temperature, which varies for different single-electron states, exceeds the superconducting gap energy.

The electron spin is of central importance in two of the most widely studied many-body phenomena in solid-state physics: the Kondo effect and superconductivity. The Kondo effect can be understood as a magnetic exchange interaction between a localized impurity spin and free conduction electrons [1]. In order to minimize the exchange energy, the conduction electrons tend to screen the spin of the magnetic impurity and the ensemble forms a spin singlet. In an *s*-wave superconductor the electrons form pairs with antialigned spins and are in a singlet state as well. When present simultaneously, the Kondo effect and superconductivity are usually expected to be competing physical phenomena. In a standard *s*-wave superconductor containing magnetic impurities, for example, the local magnetic moments tend to align the spins of the electron pairs in the superconductor which often results in a strongly reduced transition temperature. A more subtle interplay has been proposed for exotic and less well-understood materials such as heavy-fermion superconductors in which both effects might actually coexist [2].

Given the complexity of a system involving two different many-body phenomena, it would be highly desirable to have a means to investigate their mutual interplay at the level of a single impurity spin. In this respect, the study of a quantum dot as an artificial impurity in between superconducting reservoirs is of great interest. This approach has already proved very successful in the study of the Kondo effect in normal metals [3–5]. Here we achieve this for a carbon nanotube quantum dot coupled to superconducting Au/Al leads.

The device we consider consists of an individual multiwall carbon nanotube (MWNT) of 1.5 μm length between source and drain electrodes that are separated by 250 nm [6]. The lithographically defined leads were evaporated over the MWNT, 45 nm of Au followed by 135 nm of Al. The degenerately doped Si substrate was used as a gate electrode. Low-temperature transport measurements of the device exhibited pronounced superconducting proximity effects, as did all other 14 measured samples having Au/Al contacts.

Before investigating the influence of the superconducting correlations in the leads, the sample is characterized with the contacts driven normal by a magnetic field of 26 mT. This field is quite small in terms of the Zeeman energy ($g\mu_B B = 3.0$ μeV at $B = 26$ mT where μ_B is the Bohr magneton and $g \simeq 2$ the gyromagnetic ratio) but exceeds the critical field of the electrodes, which was experimentally determined to be $\sim$12 mT. Figure 1 shows a grey scale representation of the differential conductance as a function of source drain (V_{sd}) and gate voltage (V_g). An alternating sequence of truncated low-conduction "diamonds," linked by narrow ridges of high conduction, can be seen. The size of the diamonds reflects the magnitude of the addition energy ΔE_{add} which measures the difference in chemical potential of two adjacent charge states of the dot. In the constant interaction model $\Delta E_{add} = U_C + \delta E$, where $U_C = e^2/C_\Sigma$ is the single-electron charging energy, C_Σ is the total electrostatic capacitance, and δE is the single-electron level spacing [7]. Starting from an even filling number, $\Delta E_{add} = U_C + \delta E$ for the first added electron (large diamond) and U_C for the second one (small diamond). The horizontal features at $V_{sd} \neq 0$ mV truncating the large diamonds are attributed to the onset of inelastic cotunneling. From the size of the truncated diamonds we obtain $\delta E \approx 0.40$–0.70 meV. The charging energy is obtained from the size of the (faintly visible) small diamonds and yields $U_C \approx 0.45$ meV.

The high-conductance ridges are a manifestation of the Kondo effect occurring when the number of electrons on the dot is odd (total spin $S = 1/2$). The width of the Kondo resonance reflects the binding energy of the spin singlet between the spin polarized dot and the electrons in the leads and is usually described by a Kondo temperature T_K. Several of the Kondo ridges observed show a conductance saturation at the lowest temperatures and the valley between peaks has completely disappeared at $T \approx$ 50 mK, which is the base electron temperature of our dilution refrigerator. Figures 1(c)–1(e) show that the Kondo ridges follow the expected behavior such as a logarithmic increase of the linear-response conductance G below T_K, a saturation of G at $T \ll T_K$, and a linear splitting into components at $V_{sd} = \pm g\mu_B B/e$ when a magnetic field is applied.
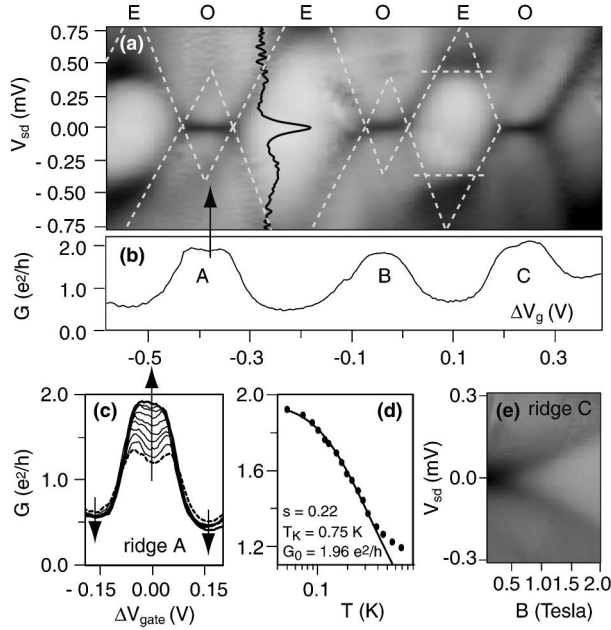
FIG. 1. (a) Grey scale representation of the differential conductance as a function of source drain (V_{sd}) and gate voltage (V_g) at $T = 50$ mK and $B = 26$ mT for a MWNT device in the Kondo regime (darker areas = more conductive). The dashed white lines outline the Coulomb diamonds. The black curve shows the dI/dV_{sd} versus V_{sd} trace at the position of the arrow. The regions with even and odd number of electrons are labeled E and O, respectively. (b) Linear-response conductance G as a function of V_g. The Kondo ridges are labeled A, B, and C. (c),(d) Temperature dependence of ridge A between 50 mK (thicker line) and 700 mK (dashed line). The data can be fitted using the empirical function given in the text yielding a Kondo temperature for ridge A of ~ 0.75 K. (e) When a magnetic field is applied (0.1–2 T), the ridges split into components at $V_{sd} = \pm g\mu_B B/e$.

From the width of the Kondo ridge out of equilibrium, the full width at half maximum (FWHM) corresponds to $\sim k_B T_K$, we estimate a Kondo temperature of 0.82 K for ridge "A" [8]. The Kondo temperature can also be obtained from the temperature dependence of the linear-response conductance. In the middle of the ridge this is given by the empirical function: $G(T) = G_0/[1 + (2^{1/s} - 1)(T/T_K)^2]^s$, where $s = 0.22$ for a spin 1/2 system and G_0 is the maximum conductance [9]. A best fit to the data yields $G_0 = 1.96e^2/h$ and $T_K = 0.75$ K, in agreement with the estimate of T_K from the width of the Kondo ridge. From here on the width of the resonance out of equilibrium is taken as the measure of T_K. For the ridges "B" and "C" this yields T_K's of 1.11 and 0.96 K, respectively.

We now turn to the behavior of the conductance when the magnetic field is switched off and the reservoirs become superconducting. Figure 2 shows a grey scale representation of the differential conductance versus V_{sd} and V_g for the same gate range of Fig. 1 at $B = 0$ mT.
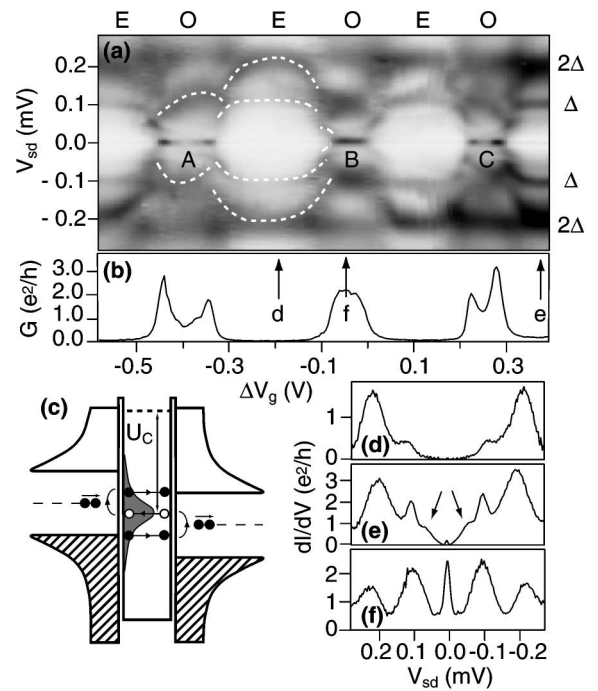

FIG. 2. (a) Grey scale representation of the differential conductance as a function of V_{sd} and V_g at $T = 50$ mK and $B = 0$ mT for the same gate region as in Fig. 1. The dotted white lines indicate the shift of the Andreev peaks. (b) Linear-response conductance G as a function of V_g. (c) Schematics (simplified) of a quantum dot between superconductors showing two Andreev reflections. (d)–(f) dI/dV versus V_{sd} for the V_g positions indicted by the arrows in panel (b).

Note that the vertical axis is shown only between -0.3 and 0.3 mV here. From comparing Figs. 1 and 2 it is clear that the conductance pattern has completely changed. The horizontal lines around $V_{sd} = \pm 0.20$ mV in Fig. 2 correspond to the superconducting gap of 2Δ, and mark the onset of direct quasiparticle tunneling between source and drain [10]. These lines continue throughout the whole measured gate range, fluctuating slightly with varying V_g, and have been observed for all 14 samples studied. The appearance of a subgap structure at $V_{sd} \leq 2\Delta$ can be understood by invoking multiple Andreev reflection (MAR) at the boundaries of the superconducting leads and the quantum dot [11,12]. Andreev reflection is a higher-order tunneling process in which an incident electron is converted into a Cooper pair, leaving a reflected hole in the normal region [see Fig. 2(c)]. Andreev reflection has been studied extensively in mesoscopic devices such as thin wires or break junctions [13] in which electron-electron interaction and energy-level quantization can be neglected.

In a quantum dot, however, Coulomb interaction cannot be neglected and is expected to suppress higher-order MAR [14,15]. It is evident from Fig. 2 that the current through the dot also crucially depends on the level position of the electron states and on the number of electrons

on the dot, having total spin $S = 0$ or $S = 1/2$. Note that both U_C, $\delta E > 2\Delta$ in the gate range of Fig. 2 and only a single level is expected to be present within a bias window 2Δ.

We will first discuss the conductance behavior in the even diamonds ($S = 0$). In the normal state the conductance has a relatively large value of $\sim 0.5e^2/h$ in the middle of the diamonds but becomes suppressed when the leads are superconducting; see Figs. 2(d) and 2(e). Whereas in the normal state second-order elastic cotunneling processes can contribute significantly to the conductance in our device, this is no longer allowed in the superconducting state due to the opening of an energy gap in the leads. Only higher-order MAR processes can give rise to a finite conductance at small bias. The dominant order n depends on V_{sd} as $2\Delta/en \leq V_{sd} \leq 2\Delta/e(n - 1)$ and is therefore large when V_{sd} is small. This leads to a rapid decay of the linear-response conductance when a single-electron state is tuned away from the Fermi energy of the leads and G almost completely vanishes in the middle of the diamonds. When V_{sd} is increased, lower-order MAR processes become possible. Indeed at $V_{sd} \approx 0.10$ mV (Δ/e) the current increases [see peaks in the dI/dV in Figs. 2(d)–2(f)], corresponding to the opening of a channel with one Andreev reflection ($n = 2$). In Fig. 2(e) peaks in the dI/dV at even lower V_{sd} can be observed (arrows), probably involving a process with two Andreev reflections ($n = 3$), shown schematically in Fig. 2(c).

It is interesting to note that, as indicated in Fig. 2(a) by the dotted white lines, the Andreev peaks appear to shift in energy as V_g is changed. This is unique for quantum dots and related to the shift of the level position of the single-electron states with V_g [16,17]. A detailed comparison of the observed energy dependence of the MAR peaks with theory is beyond the scope of this paper and will be published elsewhere.

For the odd diamonds ($S = 1/2$) the situation is different. In the normal state the source and drain electrode are strongly coupled by virtue of the Kondo effect. The lowest-order process in the normal state, where one electron on the dot is replaced by another one with opposite spin, is no longer directly possible in the superconducting state since each such process must necessarily break a Cooper pair. One might therefore expect the Kondo effect to be suppressed when the leads become superconducting. Indeed, the conductance in the middle of two of the Kondo ridges (A and C) diminishes in the superconducting state. The conductance of Kondo ridge B, however, is actually *enhanced* and a narrow resonance remains around $V_{sd} = 0$ mV; see Fig. 2(f). Note that ridge B has a higher T_K than those of A and C. These observations are in accordance with theoretical predictions which state that the Kondo resonance should *not* be destroyed by the superconductivity if T_K is sufficiently large [18–20]. More precisely, a crossover is expected for $k_B T_K \sim \Delta$.

The Kondo temperature varies from level to level reflecting the fact that the wave functions of the particular quantum states can have different overlaps with the electrodes. Since we observe a multitude of Kondo resonances in our MWNT quantum dot, having a variety of T_K's we are able to test the theoretical predictions mentioned above. The width (FWHM) of the observed Kondo ridges, corresponding to $k_B T_K/e$, ranges between 0.045 and 0.29 mV. The superconducting gap is a constant ($\Delta/e \approx 0.10$ mV), which means that the ratio of both numbers can be both slightly larger or smaller than 1 depending on the particular level. In Fig. 3 we show three different Kondo ridges with increasing T_K from left to right. The conductance in the middle of the narrowest ridge is clearly suppressed when the leads become superconducting. At the other end of the spectrum, however, a pronounced increase can be observed. This can be understood qualitatively considering that in the latter case the energy necessary to break a Cooper pair, which is proportional to Δ, is more than compensated for by the formation of the Kondo singlet, having a binding energy of $\sim k_B T_K$. The Kondo state now provides a strong coupling between superconducting electrodes and the conductance can
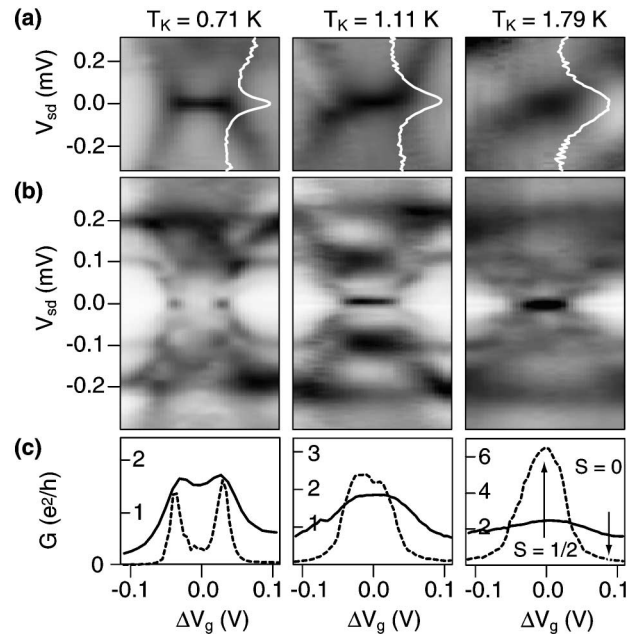

FIG. 3. (a) dI/dV grey scale plot for three different Kondo ridges at $T = 50$ mK and $B = 26$ mT. The dI/dV_{sd} versus V_{sd} traces are measured in the middle of the ridges. (b) The same plot for the superconducting state. An intricate pattern develops showing multiple Andreev peaks, the position and magnitude of which depend on the level position. (c) Linear-response conductance in the normal (solid lines) and superconducting (dashed lines) state. The rightmost plot shows that even if the conductance modulation in the normal state is weak and $G \sim 2e^2/h$ both for $S = 0$ and $S = 1/2$, the difference can be dramatic when the leads are superconducting.
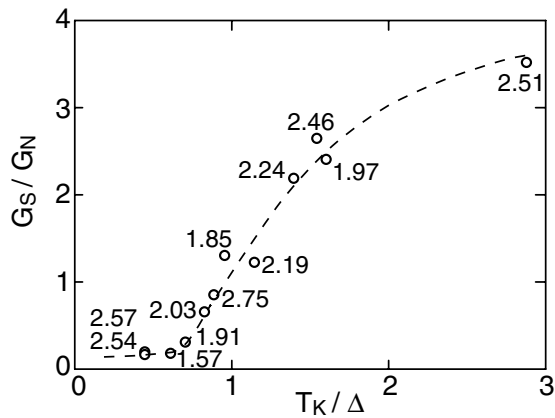
FIG. 4. The data points give the ratio G_S/G_N of the conductances in the middle of 12 different Kondo ridges in the superconducting (G_S) and normal (G_N) state versus T_K/Δ measured at $T = 50$ mK. The gap energy Δ is 0.1 meV, corresponding to 1.16 K. The numbers indicate G_N in units of e^2/h for each data point [23]. The dashed line is a guide to the eye.

increase far beyond its normal-state value [21,22]. In Fig. 4 we show the ratio of the conductances in the superconducting and normal state, G_S/G_N, versus T_K/Δ for all measured Kondo resonances. The crossover between increased and suppressed conductance indeed appears at $T_K/\Delta \sim 1$, consistent with the theoretical predictions.

The present study has shown detailed transport measurements of a carbon nanotube quantum dot coupled to superconducting leads. Exactly such systems are presently considered as excellent candidates for the creation of nonlocal spin-entangled electron pairs [24,25]. In these proposals the superconductor acts as a natural source of entangled electrons (the Cooper pairs) and the repulsive interaction in the nanotubes can be exploited to spatially separate the electrons of a pair. Future research will explore this important topic further.

---

*Electronic address: Christian.Schoenenberger@unibas.ch

[1] L. Kouwenhoven and L. Glazman, Phys. World **14**, No. 1, 33–38 (2001).

[2] D. L. Cox and M. B. Maple, Phys. Today **48**, No. 2, 32–40 (1995).

[3] D. Goldhaber-Gordon *et al.*, Nature (London) **391**, 156 (1998).

[4] S. M. Cronenwett, T. H. Oosterkamp, and L. P. Kouwenhoven, Science **281**, 540 (1998).

[5] J. Nygård, D. H. Cobden, and P. E. Lindelof, Nature (London) **408**, 342 (2000).

[6] M. R. Buitelaar, A. Bachtold, T. Nussbaumer, M. Iqbal, and C. Schönenberger, Phys. Rev. Lett. **88**, 156801 (2002).

[7] L. P. Kouwenhoven *et al.*, in *Mesoscopic Electron Transport*, edited by L. L. Sohn (Kluwer, Dordrecht, The Netherlands, 1997).

[8] Y. Meir, N. S. Wingreen, and P. A. Lee, Phys. Rev. Lett. **70**, 2601 (1993).

[9] D. Goldhaber-Gordon *et al.*, Phys. Rev. Lett. **81**, 5225 (1998).

[10] The value of $2\Delta \approx 0.20$ meV is smaller than the expected bulk value for Al which is 0.36 meV. This can be attributed to the intermediate Au layer, necessary to obtain good electrical contact between the leads and the MWNT. Similar findings were reported for measurements on break junctions consisting of an Au/Al bilayer. E. Scheer *et al.*, Phys. Rev. Lett. **86**, 284 (2001).

[11] A. F. Andreev, Sov. Phys. JETP **19**, 1228 (1964).

[12] M. Octavio, M. Tinkham, G. E. Blonder, and T. M. Klapwijk, Phys. Rev. B **27**, 6739 (1983).

[13] E. Scheer *et al.*, Phys. Rev. Lett. **78**, 3535 (1997).

[14] D. C. Ralph, C. T. Black, and M. Tinkham, Phys. Rev. Lett. **74**, 3241 (1995).

[15] A. F. Mopurgo, J. Kong, C. M. Marcus, and H. Dai, Science **286**, 263 (1999).

[16] A. Levy Yeyati, J. C. Cuevas, A. López-Dávalos, and A. Martín-Rodero, Phys. Rev. B **55**, R6137 (1997).

[17] G. Johansson, E. N. Bratus, V. S. Shumeiko, and G. Wendin, Phys. Rev. B **60**, 1382 (1999).

[18] A. A. Abrikosov and L. P. Gor'kov, Sov. Phys. JETP **12**, 1243 (1961).

[19] L. I. Glazman and K. A. Matveev, JETP Lett. **49**, 659 (1989).

[20] Y. Avishai, A. Golub, and A. D. Zaikin, cond-mat/ 0111442.

[21] A. Yu. Kasumov *et al.*, Science **284**, 1508 (1999).

[22] No supercurrent branch has been observed. We attribute this to quantum and thermal fluctuations in our device; see, e.g., A. Steinbach *et al.*, Phys. Rev. Lett. **87**, 137003 (2001).

[23] The normal-state conductance G_N can reach values as high as $2.7e^2/h$ implying that more than one level contributes to the current. Note that for an ideal nanotube with perfectly open contacts a conductance of $4e^2/h$ is expected.

[24] P. Recher, E. V. Sukhorukov, and D. Loss, Phys. Rev. B **63**, 165314 (2001).

[25] P. Recher and D. Loss, Phys. Rev. B **65**, 165327 (2002); C. Bena, S. Vishveshwara, L. Balents, and M. P. A. Fisher, Phys. Rev. Lett. **89**, 037901 (2002).